# Nonisothermal Crystallization of Polytetrafluoroethylene in a Wide Range of Cooling Rates

Nicolas Bosq,[†] Nathanaël Guigo,[†] Evgeny Zhuravlev,[‡] and Nicolas Sbirrazzuoli*,[†]

[†]Université Nice Sophia Antipolis, Laboratoire de Physique de la Matière Condensée, Equipe Fluides et Matériaux Complexes CNRS UMR 7336, Parc Valrose, 06108 Nice Cedex 2, France

[‡]University of Rostock, Institute of Physics, Wismarsche Str. 43-45, 18057 Rostock, Germany

ABSTRACT: Compared to other semicrystalline polymers, PTFE demonstrates a very fast crystallization process on cooling. This study explores for the first time the nonisothermal PTFE ultrafast crystallization under tremendously fast cooling rates (up to 800 000 K·s^{-1}) achieved by using fast scanning calorimetry (FSC) and ultra-fast scanning calorimetry (UFSC). Regular DSC was also used to get crystallization at slower rates. The data obtained on a wide range of cooling rates (over 8 orders of magnitudes) help to get new knowledge about crystallization kinetics of PTFE. Both FSC and UFSC data show that it is impossible to bypass the crystallization and thus to reach a metastable glassy state even for the fastest cooling rate employed (800 000 K·s^{-1}). The crystals formed under such conditions are slightly less stable than those produced under slower cooling rates, as reflected by a shift of the melting peak to lower temperature. The difference in crystal morphologies was confirmed by SEM observations. The variation of the effective activation energy (E_α) with the relative extent of crystallization reveals that PTFE crystallization follows a transition from regime II to regime III around 315−312 °C. Corroborated temperature dependences of E_α obtained respectively for crystallizations under slow and fast cooling rates were combined and fitted to the theoretical dependence of the growth rate derived from the Hoffman−Lauritzen theory.
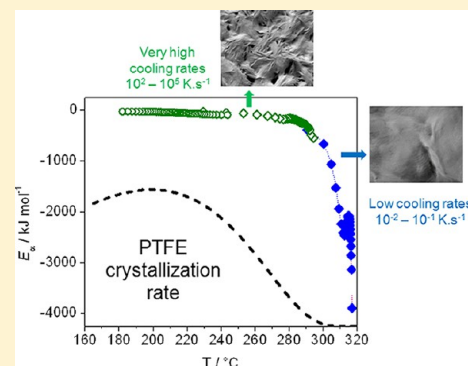
1. INTRODUCTION

Materials properties such as permeability, elasticity, toughness, or transparency strongly depend on their micromorphology that apart structural correlation is influenced by the thermomechanical history. Polytetrafluoroethylene (PTFE) is a well-known synthetic thermoplastic fluoropolymer that was originally discovered in 1938 by Roy Plunkett of DuPont De Nemour society. In PTFE, the fluorine atoms create a protective layer around the carbon skeleton. This layer protects the PTFE on chemical or thermal actions/damage and induces peculiar surface and interface properties. Its chemical inertness, thermal stability, hydrophobicity, and many other physical properties such as biocompatibility and nonadhesive properties make PTFE widely used to elaborate smart materials which are subjected to extreme conditions.[1] Due to its excellent insulating and dielectric properties, PTFE is well-suited for cable insulations and microwave applications. Widely employed in bearing and seals applications, it exhibits a low coefficient of friction and a high rate of wear.[2] It is worth noting that PTFE exhibits a high maximum use temperature (>260 °C) and a high melting point (327 °C).

As for every semicrystalline polymer, the thermomechanical history[3−5] of PTFE influences its crystallinity and crystal morphology which in turn determine the macroscopic properties such as thermal conductivity.[6] The knowledge of PTFE crystallization kinetics is of great interest to understand the structuration at a micrometric scale. PTFE is known to

crystallize faster than other semicrystalline polymers because of its higher degree of structural regularity. It must be stressed that nonisothermal conditions are generally used for real industrial processes such as melt spinning; thus, the comprehension of nonisothermal crystallization kinetics is of major significance. Ozawa[7] studied for the first time the nonisothermal crystallization kinetics of PTFE by means of differential scanning calorimetry (DSC) measurements and found a value of Avrami's coefficient $n \sim 1$, concluding that crystals grow one-dimensionally by one dimension from pre-existing nuclei. More recently, Wang et al.[8] obtained similar results using Avrami's and Ozawa's equations respectively from isothermal and nonisothermal DSC data. Seo[9] proposed an alternative approach to the Ozawa equation by taking into account the evolution of maximum peak temperature as a function of the cooling rate and found an Avrami exponent of $n \sim 1.5$ for PTFE crystallization. This value implies that both one-dimensionally and two-dimensionally grown crystallites have been developed. The former type of crystals is produced from thermal nucleation (i.e., homogeneous nucleation), while the latter is formed from athermal nucleation (i.e., heterogeneous nucleation). Lambrigger[10] defined theoretical crystallization limits and Avrami master curves for the PTFE and for isotactic

polypropylene (iPP) crystallization, respectively. The author concluded that PTFE crystallization is less symmetrically balanced compared to that of iPP. Consequently, PTFE crystallization is more sensitive to cooling-rate-dependent anomalies such as crystallite fractions formed during secondary crystallization.

The influence of various fillers on the PTFE crystallization was also investigated. Wang et al.[8] determined that glass fibers have a poor nucleation activity. Kostov et al.[11] studied the PTFE polymerization in the presence of $CaCO_3$ and showed that generated crystals from inorganic fillers have grown one-dimensionally. Secondary crystallization was not observed. Recently, Wang et al.[12] concluded that a relatively low content of solid glass microspheres promotes a heterogeneous nucleation, while a higher loading of the PTFE provokes a significantly reduced crystallization rate.

The above-mentioned investigations show clearly that PTFE crystallizes very quickly, thus limiting considerably the experimental solutions to follow up the crystallization process. DSC was routinely used to obtain experimental data on the PTFE crystallization, whereas the fastest applied cooling rates did not exceed 1 K·s^{-1} in the best case.[8] However, under very fast cooling rates, it should be theoretically possible to overcome (or at least to disturb) the ordering crystallization process and to reach a crystallization temperature range that has never been reached so far. Recently, fast scanning calorimetry (FSC) and ultra-fast scanning calorimetry (UFSC) have helped to breakthrough knowledge in the field of polymer crystallization. Their principle is based on a calorimeter chip technology. Ultrafast heating/cooling rates (>100 000 K·s^{-1}) are reached thanks to the combination of small thermal resistance of the chip with the miniscule amount of sample. This technique has given new insights on crystallization of various polymers such as iPP,[13,14] poly-caprolactone,[15,16] and polyamide[17] because the ordering process was partially or entirely suppressed under sufficiently fast cooling. To our knowledge, no FSC or UFSC studies were devoted to the PTFE crystallization.

The present study explores for the first time the non-isothermal crystallization of PTFE over very large cooling rate regions. For this purpose, conventional DSC, fast scanning calorimetry (FSC), and ultra-fast scanning calorimetry (UFSC) measurements were conducted. The original combination of these three techniques allowed studying the PTFE crystallization process on cooling for scanning rates lying in between 10^{-2} and 8×10^5 K·s^{-1}. The melting profiles will be analyzed and corroborated to direct SEM observation in order to get reliable information on the crystal perfection after each undercooling. The study provides for the first time an advanced isoconversional analysis of PTFE crystallization kinetics over a large temperature range. The obtained variations of effective activation energy, E_α, are interpreted in terms of the Hoffman–Lauritzen theory. Important changes in the crystallization mechanism over temperature are discussed hereby.

2. ADVANCED ISOCONVERSIONAL KINETIC ANALYSIS

The rate of heat release measured by DSC is assumed to be proportional to the macroscopic rate of crystallization, so that the relative extent of crystallization at time t, α_t, is computed according to eq 1

$$\alpha_t = \frac{\int_0^t (dH/dt)\,dt}{\int_0^\infty (dH/dt)\,dt} = \frac{\alpha_{c(t)}}{\alpha_{c(\infty)}} \quad (1)$$

where $\alpha_{c(t)}$ and $\alpha_{c(\infty)}$ are the extent of crystallization at time t and at the end of crystallization (time $t \to \infty$), respectively. The general form of the basic rate equation is usually written as[18]

$$\frac{d\alpha}{dt} = k(T)f(\alpha) \quad (2)$$

where $f(\alpha)$ is the function that represents the reaction model related to the crystallization mechanism. Arrhenius law gives the dependence of the rate coefficient with temperature:

$$k(T) = A e^{-E/RT} \quad (3)$$

where E is the activation energy, A is the pre-exponential factor, and R is the universal gas constant.

To overcome the drawbacks of integral methods and to take into account the variation of E in the computation of the temperature integral, advanced isoconversional methods have been developed.[19,20] As with conventional isoconversional methods, the advanced isoconversional method allows one to calculate the effective activation energy, E_α, for each value of the relative extent of crystallization α. In the case of a single-step process, E_α is constant, while complex (i.e., multistep) kinetics will reveal an E_α variation that can be meaningful for treating process complexity. Isoconversional kinetic analysis applied to dynamic DSC data is a powerful concept for disclosing and handling the complexity of thermally stimulated processes and to obtain important information on the related mechanisms.[21]

The E_α value is fixed as the value that minimizes the function[22]

$$\Phi(E_\alpha) = \sum_{i=1}^{n} \sum_{j \neq i}^{n} \frac{J[E_\alpha, T_i(t_\alpha)]}{J[E_\alpha, T_j(t_\alpha)]} \quad (4)$$

where J is evaluated over small intervals of E variation

$$J[E_\alpha, T_i(t_\alpha)] \equiv \int_{t_{\alpha-\Delta\alpha}}^{t_\alpha} \exp\left[\frac{-E_\alpha}{RT_i(t)}\right] dt \quad (5)$$

This method can be applied to any temperature program and uses a numerical integration of the temperature integral. The resulting advanced isoconversional method allows one to handle a set of n experiments carried out under different temperature programs, $T_i(t)$. The software developed by Sbirrazzuoli[23] was used to compute a value of E_α for each value of α lying in between 0.02 and 0.98 with a step of 0.02. Numerical integration was performed using the trapezoidal rule. An accurate interpolation of the integrated $\alpha-T$ curves was performed using a Lagrangian algorithm to find the time $t_{\alpha,i}$ and temperature $T_{\alpha,i}$ that correspond to a given α for the i temperature programs used. The precision on the determination of the time to reach a given α value was extended for FSC measurements. The same Lagrangian algorithm was also applied to increase the number of points of FSC data recorded for fast crystallization of PTFE. Several possibilities are proposed in this software for the initial estimate E_0 for E_α in the nonlinear procedure corresponding to Vyazovkin's equation. The first possibility is based on the assumption that $\Phi(E_\alpha)$ can be approximated by a quadratic parabola with an interval of variation of E_α typically lying in between 1 and 400

kJ·mol^{-1} as initially proposed by S. Vyazovkin.[19] On the other hand, employing this software, it is also possible to use the E_α values obtained by the Friedman method[23] as an initial estimate of E_α or to use an iterative computational procedure between extreme values (-5000 and $+5000$ kJ·mol^{-1} for example). This last procedure being used in this study has been developed to be applicable for strong E_α variations and apparent "negative" values, as obtained in the case of thermoplastic crystallization (anti-Arrhenius behavior).[24] In the present study, this computation is referred to as the nonlinear method (NLN).

3. MATERIALS AND METHODS

PTFE with micrometric particle powder size was purchased from Aldrich Chemical Co. (Aldrich number 430935, m.p. = 321 °C) and was used as received. DSC runs were carried out on a heat flux Mettler-Toledo DSC 1. Temperature, enthalpy, and tau lag calibrations were steadily done by using indium and zinc standards. The PTFE sample ($\sim$4 mg) was placed in 40 μL aluminum crucible hermetically sealed, and the experiments were performed under a N_2 atmosphere (80 mL·min^{-1}). The PTFE equilibrium melting temperature deduced from the Hoffman–Weeks routine was experimentally determined to be around T_m° $\sim$324 °C. All the DSC runs were conducted in a similar way. First, the PTFE sample was heated at 360 °C (i.e., T_m° + 36 °C) for 5 min to reach the molten state and erase the thermal history. Then, the sample was undercooled from 360 to 100 °C at the following cooling rates: 1, 2, 5, and 20 K·min^{-1} (respectively 0.0167, 0.0334, 0.0834, and 0.334 K·s^{-1}).

Fast scanning calorimetry (FSC) was performed on the Mettler-Toledo Flash DSC1 using the UFS1 chip calorimeter. More details about the instrumental setup and chip calibration can be found elsewhere.[25,26] Each sensor has a specific serial number and is calibrated by Mettler-Toledo. Then, this number is entered in the STAR software for data treatment. Calibration is then checked by using indium samples. Various experiments were realized using different sample masses. If two experiments with different sample masses lead to the same thermograms, then it was considered that the thermal lag inside the sample is negligible. No thermal lag correction was applied. To run FSC experiments, some PTFE particles were placed directly on the sample area of the sensor while the reference area remains free. Repetitive heating and cooling scans were performed to melt and crystallize the PTFE sample, several times, in order to obtain a uniform sample that remains stuck to the sensor. The mass of the sample was about a few nanograms and was quantitatively obtained by the normalization of the melting peak obtained in FSC (J) with the melting peak obtained in DSC (J·g^{-1}). In both cases, the PTFE samples were previously crystallized via the same cooling program (0.334 K·s^{-1}) to have comparable crystalline parts.

Ultra-fast scanning calorimetry (UFSC) was performed on a calorimeter described elsewhere.[27,28] It is similar to the Mettler-Toledo Flash DSC but employs a smaller working area and thinner (0.5 μm vs 2 μm) membrane film sensors, designed for fast temperature scanning rates. The device operates in the 10–1000 K temperature window and can realize both heating and cooling from 1 to 2 000 000 K/s. Reliable heat flow measurement can be performed in range of scanning rates from 100 to 500 000 K·s^{-1}. Due to the limited cooling rate range coverage of a particular sensor size, two different sensors were used in this work. The average sized 60 × 60 μm^2 sensor (XEN-39269) realized cooling from 100 to 500 000 K·s^{-1}. The sensor (XEN-39292) with working area as small as 8 × 10 μm^2

was able to control the sample temperature on cooling up to 2 000 000 K·s^{-1}. For better scanning rate performance, the sample was measured in a helium atmosphere at reduced pressure (40 mbar). Liquid nitrogen cooling was used to keep the sensor housing at 80 K. The mass of the sample can be estimated from the heat capacity in the liquid state and the specific heat capacity, measured by conventional DSC.

As for DSC, all the FSC runs were started by first melting the samples at 360 °C for 30 s to erase the thermal history. Then, the samples were cooled down from T_1 = 360 °C to T_2 = 100 °C at different cooling rates ranging from 0.1 to 5000 K·s^{-1}. The α relaxation temperature of the PTFE paracrystalline phase (sometimes associated to T_g) fractions is around 135 °C. At T_2 = T_g − 35 °C, no structural changes are likely to occur in the material. At 100 °C, a waiting period of 0.1 s was fixed for stabilization of the calorimeter. After this waiting period, the samples were heated at 1000 K·s^{-1} to 360 °C. Then, the observed changes in the melting peak were attributed to the previous cooling segment. For the UFSC runs, the samples were cooled between 430 and −173 °C. The sample was at the highest temperature for 0.01 s to avoid degradation.

The crystallization temperature was arbitrarily chosen as the peak maximum temperature and was measured for the different cooling scans obtained by DSC and FSC. For FSC measurements, melting was estimated on the heating segment consecutive to nonisothermal crystallization on cooling. Temperature (also chosen as the peak maximum temperature) and enthalpy of melting were obtained for PTFE crystals formed under various cooling rates. An advanced isoconversional method was applied to nonisothermal crystallization of PTFE measured with regular DSC (cooling rates ranging from 0.0167 to 0.334 K·s^{-1}), FSC (500 to 5000 K·s^{-1}), and UFSC (40 000 to 800 000 K·s^{-1}). The resulting E_α dependencies were analyzed in order to gain information on the mechanisms of crystallization.

The crystal morphologies of the PTFE samples have been investigated by scanning electron microscopy (SEM) at the Microscopy Centre of University Nice Sophia Antipolis. The SEM apparatus was a JEOL 6700F microscope equipped with a field emission gun. The electron beam voltage was fixed to 1 kV. The samples were mounted on the microscope studs using silver colloidal paste and sputter coated with gold palladium.

4. RESULTS AND DISCUSSION

Figures 1 and 2 present, respectively, the variation of apparent heat capacity (i.e., heat flow divided by cooling rate) and relative extent of crystallization (obtained by integration of calorimetric data) measured during nonisothermal crystallization of PTFE from the melt. The presented thermoanalytical curves gather data obtained at slow and very fast cooling rates by means of DSC, FSC, and UFSC measurements, respectively. Figure 1 shows that the crystallization peak is shifted to lower temperature with increasing cooling rate. It must be stressed that the exothermal crystallization peak is not symmetrical at slow cooling rate. This asymmetry is also shown in the relative extent of crystallization (Figure 2). This trend was already observed by several authors[7,9,12] and was explained by a transition from a primary to a secondary crystallization process. At faster cooling rates, the peak is more symmetrical, which would indicate that the secondary crystallization process is limited.

For the fastest cooling rates used in this study (up to 8 × 10^5 K·s^{-1}), most of the common thermoplastics would have been
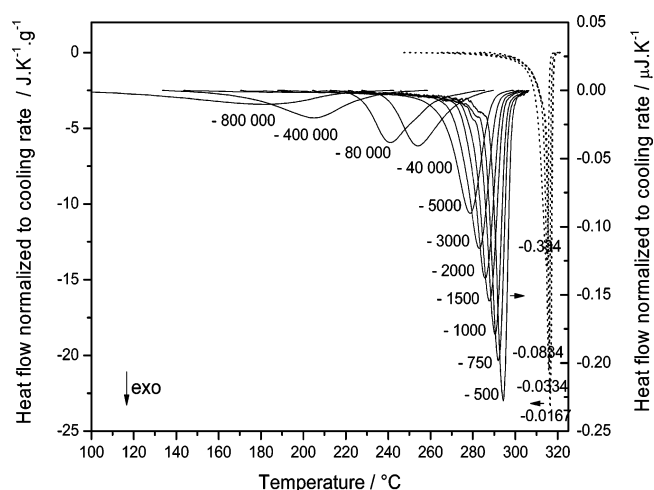
Figure 1. DSC (dot) and FSC+UFSC (line) heat flow normalized to cooling rate for nonisothermal crystallization of PTFE melt at different cooling regimes. The numbers by the lines represent the rate in $K \cdot s^{-1}$.
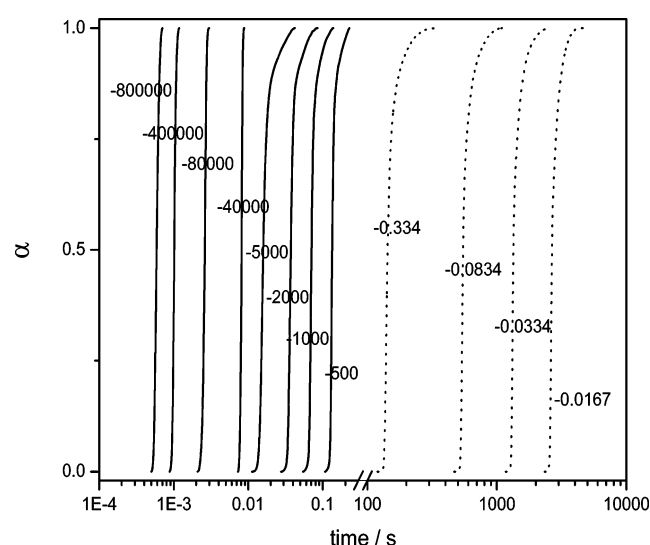

Figure 2. Integral DSC (dot) and FSC+UFSC (line) data for nonisothermal crystallization of PTFE melt at different cooling rates. The numbers by the lines represent the rate in $K \cdot s^{-1}$.

quenched in the glassy state. According to Gradys et al.,[29] the exothermic peak of crystallization of polypropylene (PP) disappears over 600 $K \cdot s^{-1}$. Concerning the polycaprolactone (PCL), the crystallization on cooling vanishes for rates faster than 300 $K \cdot s^{-1}$.[16] In the case of PTFE, the crystallization peak is continuously shifted to lower temperature but never vanishes even at very fast cooling rate. It attests for very fast homogeneous and heterogeneous nucleation processes which allow formation of PTFE crystals. At maximal cooling rate, a calorimetric signal is still recorded at $T \sim 230-240$ °C with FSC. This value falls to 100 °C using UFSC at 8×10^5 $K \cdot s^{-1}$. It can be assumed that there is still sufficient molecular mobility to generate the ordering process. Crystallization is commonly centered between the melting temperature (T_m) and T_g. In the PTFE situation, the significant difference between these two temperatures (>200 °C) enables crystallization on a large temperature range. When the sample temperature is close to the melting temperature, the crystallization is controlled by the nucleation process, but it should become diffusion controlled

when the temperature decreases and reach the glass transition temperature.

Figure 2 shows the time scales necessary to crystallize the PTFE samples at different cooling rates. The nonisothermal crystallization time decreases over 7 orders of magnitude (from 2×10^3 to 5×10^{-4} s) spanning from slow to fast cooling rates. Note that the relative extents of crystallization obtained for each cooling rate do not overlap with each other, which is an important prerequisite for accurate isoconversional kinetic computations.

The variation of the crystallization peak temperature with cooling rates is presented in Figure 3. For FSC and UFSC
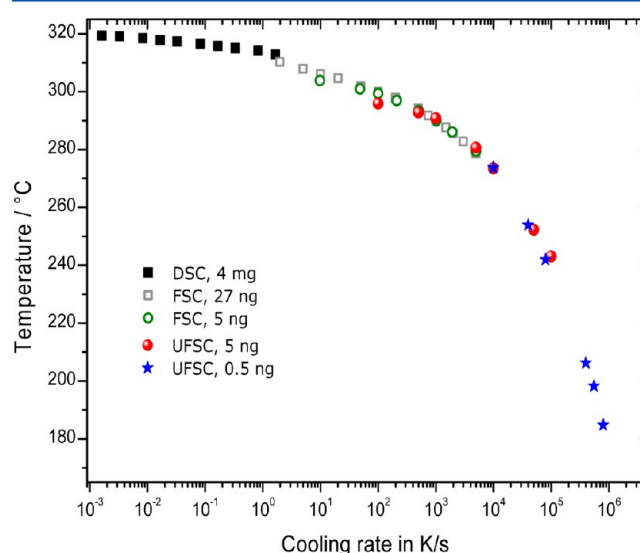

Figure 3. Crystallization peak temperature as a function of cooling rate (in absolute value) measured by DSC and FSC+UFSC. DSC data: solid squares (~4 mg). FSC: open gray squares (~27 ng) and open green circles (~5 ng). UFSC: red solid circles (~5 ng) and blue stars (~0.5 ng).

measurements, sample mass variation does not induce dramatic changes. A difference of about 135 °C is observed between extreme cooling rates. This result is in good agreement with the observation of the thermoanalytical curves in Figure 1. The crystallization proceeds at lower temperature and on a shorter time period (Figures 2 and 3) with increasing cooling rate. This necessarily suggests that the shape and the size of the formed crystals will be different and function of the cooling conditions. The crystal perfection can be indirectly correlated to their melting temperature and enthalpy. For the different crystal species formed under varying cooling conditions, the FSC enables one to compare their melting temperature and enthalpy measured on the reheating scans at 1000 $K \cdot s^{-1}$. The values are gathered in Figure 4, and some melting peaks are depicted in Figure 5. It should be mentioned that no exothermic variation was observed on heating even for samples that were previously cooled very quickly. This confirms that the sample only crystallizes on cooling. As expected, the temperature and enthalpy of melting decrease linearly with the logarithmic increase of cooling rate absolute value. This indicates that the size and perfection of the crystals are lower when the cooling rate increases. At fast cooling rate, one single melting peak is observed on the reheating scans (Figure 5) which corresponds to one type of crystalline structure. During fast crystallization, the crystals do not have enough time for thickening and
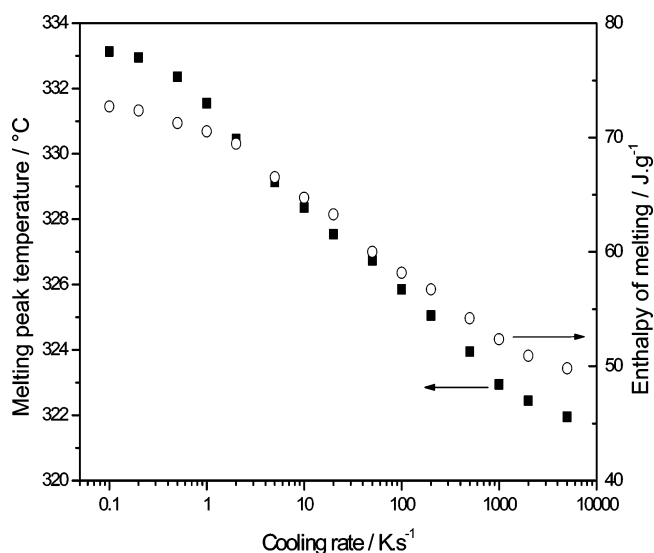
Figure 4. Peak temperature (left-hand axis) and enthalpy (right-hand axis) of melting as a function of the previous cooling rate (in absolute value) measured on heating by FSC at 1000 K·s^{-1}.
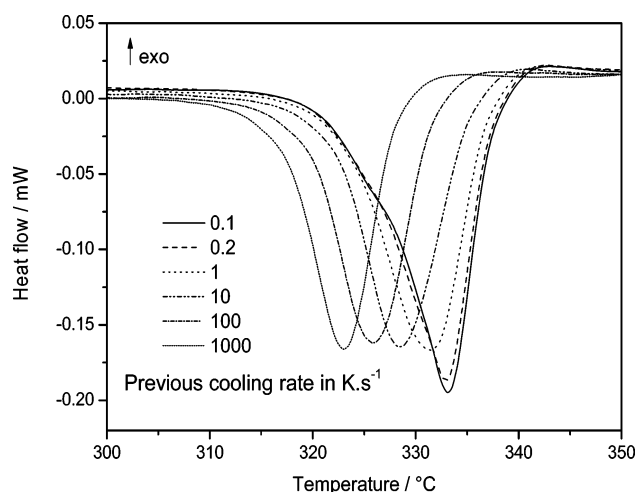

Figure 5. Melting peak obtained by FSC at 1000 K·s^{-1}. The numbers by the lines represent the crystallization cooling rate in K·s^{-1}.

Figure 6. SEM micrographs of PTFE crystals: (a) quenched from 360 °C; (b) cooled at 0.1 K·s^{-1} from 360 °C.

reorganization, which lead on heating scans to lower temperatures and enthalpy of melting. On the other hand, the crystals produced from the slow crystallization process (i.e., cooling rate <1 K·s^{-1}) present two melting structures. As shown in Figure 5, the shoulder observable on the melting peak is an indication that two crystallization processes have occurred. The low-temperature side of the peak corresponds to the melting of initially growing crystals, while the more prominent high-temperature side of the peak is rather associated to the more stable crystalline structure formed during secondary crystallization.

SEM observations were done on PTFE crystals in order to corroborate the above-mentioned differences in melting peak temperature with morphological aspects. Two samples were prepared under different nonisothermal cooling regimes. Figure 6a corresponds to the PTFE crystalline structure obtained after very fast cooling. The samples were quenched from the melt with liquid nitrogen. The resulting melting peak temperature measured at 1000 K·s^{-1} is about 326 °C. According to the data in Figure 4, the cooling regime corresponding to the quenching

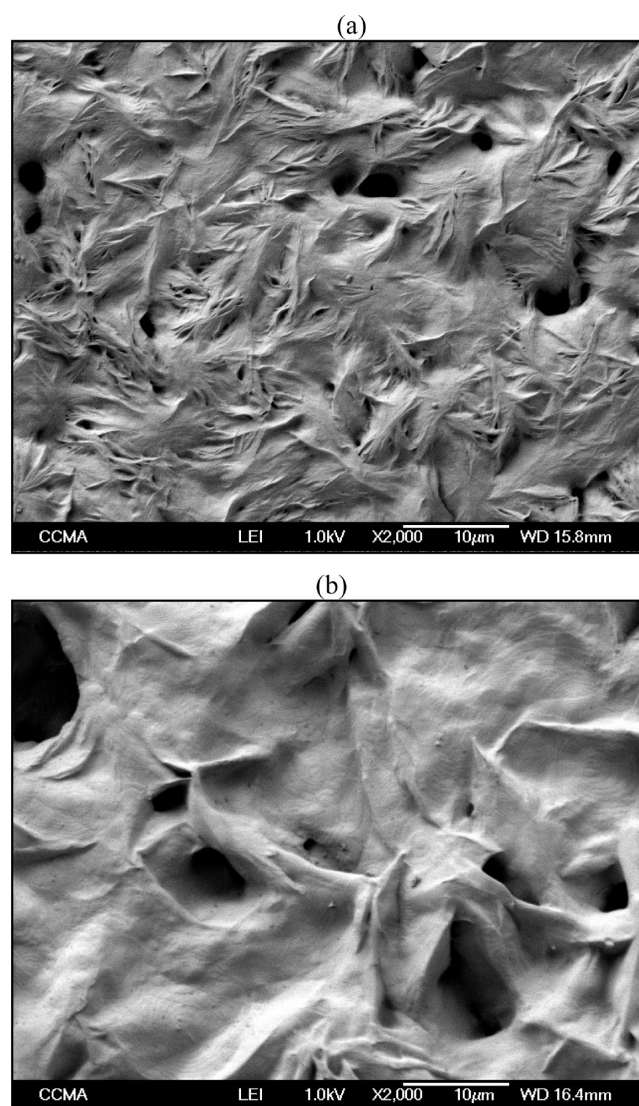condition is about 100 K·s^{-1}. Only rod-like or needle-like crystals are noticed in this case. No two-dimensional crystallites have developed. Under fast cooling, the crystals do not have enough time to rearrange and to perfect their structures and only one-dimensional growth mechanisms occur. These axialite type crystals formed under fast cooling exhibit low melting temperatures, as shown in Figure 5.

The second sample was slowly cooled at 0.1 K·s^{-1} from 360 °C. As shown in Figure 6b, the PTFE crystal exhibits ribbon-like structures that mostly arrange into concentric discs. The crystal morphologies formed under slow cooling are dramatically different from those obtained under very fast cooling rate. The discs are formed from the (slow) two-dimensional arrangements of the ribbon-like crystals. These observations would explain the peculiar melting peaks obtained after cooling at 0.1 K·s^{-1} (Figure 5). The high temperature side of the peak would correspond to the melting of the more organized two-dimensional discs. The individual ribbon-like structures are less stable than the discs and would melt at lower temperature. This is clearly observed by the shoulder observed on the low-temperature side of the peak. The different crystal morphol-

ogies shown in Figure 6 are in agreement with PTFE crystalline structures observed in previous studies.[3,5,30]

Advanced isoconversional kinetic analysis was applied to nonisothermal PTFE crystallization data measured with regular DSC, FSC, and UFSC. The resulting E_α dependencies are presented in Figure 7. Isoconversional methods describe the
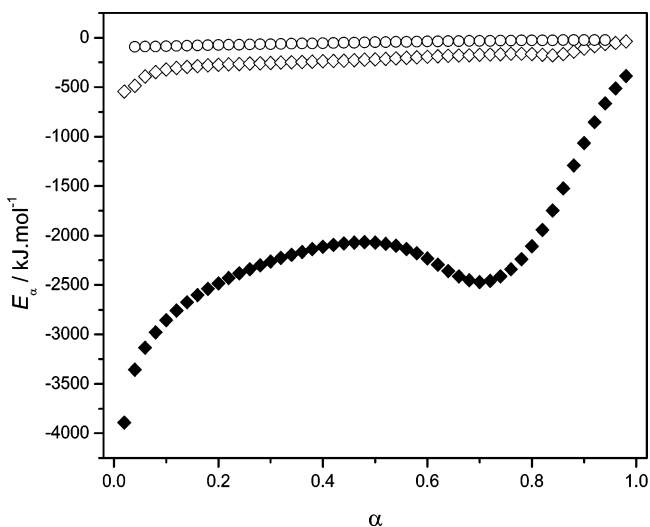

Figure 7. Dependence of the effective activation energy on the relative extent of crystallization determined by the advanced isoconversional NLN method. Solid diamonds: DSC (cooling rates: 0.0167, 0.0334, 0.0834, and 0.334 K·s^{-1}). Open diamonds: FSC (cooling rates: 500, 750, 1000, 1500, 2000, 3000, and 5000 K·s^{-1}). Open circles: UFSC (cooling rates: 40 000, 80 000, 400 000, 550 000, and 800 000 K·s^{-1}).

overall kinetics by multiple Arrhenius equations having their own E_α values, each of which is related to a certain temperature interval.[21] The existence of E_α dependence on α indicates that the effective activation energy of the process is temperature dependent. As shown in Figure 7, the E_α values associated with PTFE crystallization increase with α from around −3893 to −386 kJ mol^{-1} for nonisothermal DSC data and from around −540 to −23 kJ mol^{-1} for nonisothermal FSC and UFSC data. This effective "activation energy" does not have the usual meaning of an energy barrier in this case but simply reflects the temperature dependence of the temperature coefficient of the crystallization rate. This perfectly corroborates the assumption that the effective activation energy of the process is temperature dependent. The crystallization temperature ranges covered by DSC and FSC data are very different, which leads to different E_α dependencies. Nevertheless, the values are not randomly distributed. In both cases, it can be noticed that the negative E_α values are continuously increasing with α. Vyazovkin and Sbirrazzuoli reported a similar increasing negative dependency for polyethylene terephthalate (PET) crystallization.[24] Since this pioneering work, other authors have reported similar variations.[31,32] The negative values simply indicate that the crystallization rate decreases with increasing temperature. The crystallization process on cooling has an anti-Arrhenius behavior.

The strong dependence of E_α as a function of the relative extent of crystallization clearly indicates that PTFE crystallization on cooling from the melt is a complex process that involves several temperature-dependent steps such as nucleation and growth. The E_α dependency resulting from DSC data (Figure 7) shows a typical increase with a first maximum

around $\alpha \sim 0.48$ which corresponds to a mean temperature of 315.0 °C and a E_α value of $\sim$ −2068 kJ·mol^{-1}, and with a clear-cut break around $\alpha \sim 0.70$, which corresponds to a mean temperature of 312.6 °C and a E_α value of $\sim$ −2472 kJ·mol^{-1}. This break might be associated with the transition from a different crystallization kinetic regime. According to the Hoffman−Lauritzen theory, regime I is strongly dependent on the nucleation rate because the primary lamella is formed from a single nucleus and grows linearly. As one passes through the regime I → II transition, it leads to a downward break in the crystallization growth rate because the rate of substrate completion becomes approximately of the same order as the surface nucleation rate during regime II. At higher supercooling, the surface nucleation rate becomes very fast and the rate of crystal growth is then governed by the rate of substrate completion. This latter kinetic regime is commonly called regime III. The regime II → III transition is accompanied by an upswing break in the growth rate curve. As shown in Figure 7, E_α resulted from DSC data increases more rapidly after the break at $\alpha \sim 0.70$ which would be consistent with a transition from regime II to regime III. A similar behavior on E_α dependency has already been reported for PET crystallization[24] and has been associated with a change in the crystallization kinetic regime from a nucleation controlled rate to a crystal growth controlled rate.

The E_α dependency calculated from FSC and UFSC data shows a monotonous increase without breaks. It indicates that transition from a different crystallization kinetic regime is not observed in this case. Moreover, the absolute E_α values are significantly lower than those obtained for DSC data and tend to zero at the end of the crystallization process. It means that the nucleation rate which has a negative temperature coefficient becomes faster at fast cooling rate compared to slow cooling rates. This can be explained because the crystallization peak moves to lower temperatures when the cooling rate increases (Figures 1 and 2). Then, the nucleation rate becomes faster at lower temperature. Continuity is observed between E_α values computed from DSC, FSC, and UFSC measurements (the last E_α values computed from DSC data correspond to the first values computed with FSC, and the last E_α values computed from FSC data correspond to the first values computed with UFSC).

In order to better highlight the continuity between DSC, FSC, and UFSC kinetic data, the three E_α dependences were plotted in Figure 8 as a function of temperature. As already mentioned, the temperature coefficient (E_α) increases with T from around −3893 to −386 kJ mol^{-1} for DSC data, from −540 to −40 kJ mol^{-1} for FSC data, and from −92 to −23 kJ mol^{-1} for UFSC data. Because crystallization from the melt shifts to lower temperature with increasing cooling rate, the E_α dependences are associated with a different temperature range. For DSC data, the temperature range lies between 317.0 and 291.0 °C, while it is between 294.5 and 230.0 °C for FSC data and between 244.0 and 185.0 °C for UFSC data (temperatures corresponding to $\alpha = 0.02$ and $\alpha = 0.98$). Thus, complementary data obtained from these three techniques give a unique opportunity to compute E_α values on a very wide temperature range lying from 317 to 185 °C and to get new information on the crystallization mechanism. This region would have been limited between 317 and 290 °C with regular nonisothermal DSC data and to a temperature range of 15−20 °C using regular isothermal DSC data. Variation of the crystallization temperature coefficient (E_α) with temperature as shown in
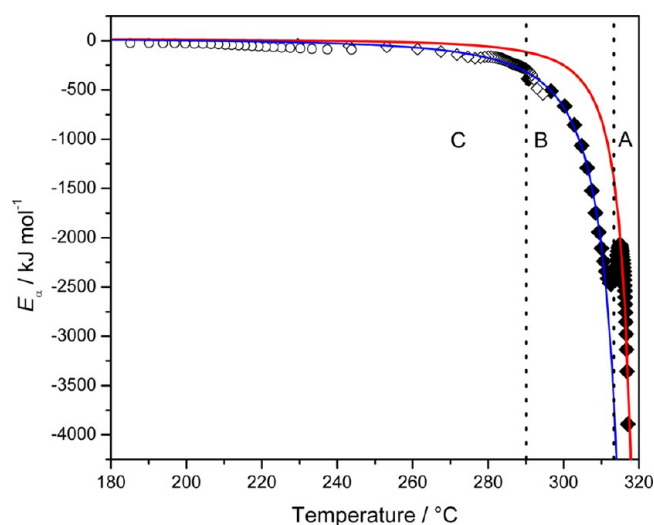
Figure 8. Dependence of the effective activation energy on average temperature (mean temperature over the cooling rates) determined by the advanced isoconversional NLN method. Solid diamonds: DSC (cooling rates: 0.0167, 0.0334, 0.0834, and 0.334 K·s⁻¹). Open diamonds: FSC (cooling rates: 500, 750, 1000, 1500, 2000, 3000, and 5000 K·s⁻¹). Open circles: UFSC (cooling rates: 40 000, 80 000, 400 000, 550 000, and 800 000 K·s⁻¹). The blue and red lines represent fits of eq 9, respectively, to region B−C and region A−C.

Figure 8 can be explained by the Hoffman−Lauritzen theory that describes the temperature dependence of the growth rate measured microscopically.[33] According to this theory, the crystallization rate passes through a maximum for a given temperature, T_{max}. If the crystallization temperature T_c lies within the region $T_{max}-T_m$, the sample will follow the anti-Arrhenius behavior that is characterized by negative values of the temperature coefficient represented here by the effective activation energy (E_α). The crystallization rate is controlled by a nucleation rate whose temperature coefficient is negative. Below T_{max}, one should observe the regular Arrhenius behavior that is characterized by positive values of the temperature coefficient. The rate becomes controlled by diffusion which has a positive temperature coefficient. This should correspond to positive values of the effective activation energy (E_α) computed by an advanced isoconversional method. According to this theory, the effective activation energy at the temperature of maximum crystallization rate T_{max} is close to zero.[24]

As shown in Figure 8, there is a perfect continuity between the dependencies computed with DSC, FSC, and UFSC data. Changes in the shape of the E_α dependency can be associated with a change in the overall crystallization mechanism. Three different portions can be highlighted in the E_α dependency vs T of Figure 8. The first region (A) lies in between 320 and 312 °C and corresponds to temperatures close to the equilibrium melting temperature. In this region, formation of stable nuclei is rate determining, and it explains why the absolute E_α values are very high and tend to decrease. As explained above, the break observed around 315−312 °C corresponds to a change in the crystallization mechanism and would be associated with a transition in a different kinetic regime. Then, the second region (B) between 312 and 290 °C corresponds to a temperature range further from T_m where nucleation occurs faster and crystallization is rather governed by crystal growth. Finally, the third region (C) below 290 °C corresponds to a temperature range far from T_m where the nucleation rate is very fast and

becomes less determining than the velocity at which the surface nucleus spreads on the crystal surface. The absolute E_α values decrease monotonously and reach very low values ($|E_\alpha| = 23$ kJ·mol⁻¹) around 185 °C. This temperature should be close to the temperature of maximum crystallization rate T_{max}, where the crystallization starts to become controlled by diffusion according to the Hoffman−Lauritzen theory.[33] The continuously increasing crystallization rate with decreasing temperature is in agreement with the crystal morphologies observed in Figure 6. The crystals which were formed under very fast cooling rate, i.e., at temperature ranges corresponding to region C, exhibit one-dimensional rod-like or needle-like structures (Figure 6a). In this case, nucleation is very fast and crystal growth is determining, which explains the formation of not extended one-dimensional axialites. On the contrary, the crystals formed at slower rate, i.e., at higher temperature (regions A and B), exhibit more complex crystalline structures such as a concentric arrangement of ribbons (Figure 6b). The nucleation rate competes with the crystal growth rate in this temperature range, which explains such two-dimensional arrangements.

The increases observed for regions A, B, and C (Figure 8) differ by the amplitudes of their slopes, so that it can be assumed that they are related to a change in the crystallization rate, probably associated with a change in crystallization mechanism. According to the isoconversional principle derived from eq 3 (the subscript α indicates the values related to a given extent of conversion)

$$\left[\frac{\partial\ln(d\alpha/dt)}{\partial T^{-1}}\right]_\alpha = -\frac{E_\alpha}{R} \tag{6}$$

the overall crystallization rate decreases when the temperature increases (anti-Arrhenius) because E_α is negative, leading to a positive value of E_α/R in eq 6. When the temperature raises T_{max}, the slope tends to be zero. This point corresponds to the transition between anti-Arrhenius and Arrhenius behavior. However, E_α never reaches a positive value, which means that the crystallization rate does not become fully controlled by diffusion.

The Hoffman−Lauritzen theory gives a dependence of the linear growth rate, G, on temperature, T, that can be expressed as

$$G = G_0 \exp\left(\frac{-U^*}{R(T - T_\infty)}\right)\exp\left(\frac{-K_g}{T\Delta Tf}\right) \tag{7}$$

where G_0 is the preexponential factor, U^* is the activation energy of the segmental jump (associated with the diffusion process), T_m is the equilibrium melting temperature, $\Delta T = T_m - T$ is the undercooling, $f = 2T/(T_m + T)$ is the correction factor, and T_∞ is a hypothetical temperature where motion associated with viscous flow ceases that is taken 30 K below the glass transition temperature, T_g. The kinetic parameter K_g associated with the nucleation process has the following form:

$$K_g = \frac{nb\sigma\sigma_e T_m}{\Delta h_f k_B} \tag{8}$$

where b is the surface nucleus thickness, σ is the lateral surface free energy, σ_e is the fold surface free energy, T_m is the equilibrium melting temperature, Δh_f is the heat of fusion per unit volume of crystal, k_B is the Boltzmann constant, and n

takes the value 4 for crystallization regimes I and III and 2 for regime II.

The parameters of the Hoffman−Lauritzen equation[33] can be evaluated by fitting the resulting E_α vs T dependence to the following equation, according to the method proposed by Vyazovkin and Sbirrazzuoli:[34]

$$E_\alpha(T) = U^* \frac{T^2}{(T - T_\infty)^2} + K_g R \frac{T_m^2 - T^2 - T_m T}{(T_m - T)^2 T} \qquad (9)$$

where U^* and K_g are the parameters associated with diffusion and nucleation.

The choice of the hypothetical temperature where motion associated with viscous flow ceases (T_∞) is essential especially for the U^* value. Molecular motions in PTFE have been studied by different techniques and are sometimes subject to debate.[35−37] The α relaxation temperature of the paracrystalline phase, i.e., the amorphous phase in the vicinity of PTFE crystals (sometimes associated with T_g), is around 135 °C. PTFE crystals exhibit well-known first-order conformational changes in crystalline structures at respectively 19 °C (triclinic → hexagonal) and 30 °C (hexagonal → pseudohexagonal), which means that there is still substantial molecular motion in this temperature range. Moreover, γ relaxation assigned to small segment mobility of the amorphous phase occurs at lower temperature (around −70 °C). Then, T_∞ was taken here at ∼ −100 °C where no conformational changes are likely to occur below this temperature.

The dependencies of E_α vs T of Figure 8 were fitted to eq 9 using the Origin 8.5 software. In order to compare the K_g value, U^* was first fixed to 6270 J·mol^{-1}. The nonlinear fitting was first performed in regions B and C of the experimental E_α dependency (Figure 8). The value of T_m is 597 K, and T_∞ is taken to be 173 K. The fit yields the values of $K_{g(BC)} = 8.7 \times 10^4$ K^2 for the temperature range 310−185 °C. From a statistical point of view, the fit is quite satisfactory. The correlation coefficient is $r^2 \sim 0.996$, while the confidence interval for $K_{g(BC)}$ is ∼0.6%. Despite the break, a nonlinear fit was performed between the temperature dependence of portions A and C without taking into account the data of region B. The fit gives $K_{g(AC)} = 3.3 \times 10^4$ K^2. Although lower than that for the BC region, the goodness of the fit remains satisfactory with $r^2 \sim 0.984$ and the confidence interval for K_g is ∼1.1%. It is interesting to remark that $K_{g(BC)}$ is approximately 2.6 times larger than the value of $K_{g(AC)}$. It is in good agreement with the theoretical ratio of $K_{gIII}/K_{gII} = 2$ between regimes II and III. It would confirm that the break observed around 315 °C on E_α vs T of Figure 8 corresponds to the regime II → III transition. On the basis of morphological studies, several authors have already highlighted the absence of the regime I → II transition and the sole presence of the regime II → III transition for high molecular weight iPP,[38] poly(ethylene succinate),[39] and poly(pivololactone).[40] Concerning PTFE, only Wang et al.[8] reported a K_g value of 1.5×10^4 K^2 using isothermal DSC data and the standard value of 6270 J·mol^{-1} for U^*. Their K_g value is different than our values because their calculations were achieved on a shorter temperature range, but both values are of same order.

When the U^* value is not set as 6270 J·mol^{-1}, then the fit for regions B and C yields to $K_{g(BC)} = 8.7 \times 10^4$ K^2 (confidence interval ∼0.8%) and $U^*_{(BC)} = 5850$ J·mol^{-1} (confidence interval ∼37%), while the goodness of the fit ($r^2 \sim 0.995$) remains unchanged. It is interesting to remark that in this case the K_g

value is practically not affected and the U^* value is close to the universal value of 6270 J·mol^{-1}.

Either for region AC or region BC, it must be stressed here that three temperature dependences of activation energy resulted from respectively DSC, FSC, and UFSC data were fitted by one single fitting curve. Indeed, fast and slow crystallization processes can be satisfactorily described with a single set of K_g and U^* parameters on time scale ranging from 10^{-4} s (UFSC data) to 10^3 s (DSC data). It means that the PTFE crystallization kinetics share common dynamics on a very large time scale, which has never been reported before for this type of polymer. A similar phenomenon has been recently described for gelation kinetics of gelatin gels where atypical and regular gelation processes share common dynamics, although they occur on significantly different time scales.[41]

While extended thanks to the use of FSC and UFSC, the available experimental temperature range (317−185 °C) does not allow observing positive E_α values (Arrhenius behavior). Since it is not possible to avoid PTFE crystallization on cooling, the E_α dependency cannot be computed on heating for cold crystallization data as was done for PET. In the case of PET, this has led to the possibility of obtaining positive E_α values corresponding to the region where the crystallization rate follows an Arrhenius behavior.[34,42] On the contrary, PTFE definitely behaves like highly flexible semicrystalline polymers such as PE which readily crystallize on cooling whatever the quenching regime. The high nucleation density mostly driven by heterogeneous nuclei leads to a continuously increasing crystallization rate that never becomes dependent on chain transport (e.g., diffusion).

The Hoffman−Lauritzen parameters K_g and U^* previously determined for the second and third regions (B and C) of the $E = f(T)$ curve ($K_{g(BC)} = 8.7 \times 10^4$ K^2 and $U^*_{(BC)} = 5850$ J·mol^{-1}) have been used to compute the dependence of the growth rate G on temperature T according to eq 7. Figure 9 shows the representation of the exponential terms contributing to the temperature dependence of the nucleation rate G. A value of the temperature of maximum crystallization rate $T_{max} \sim 200$ °C is obtained using this equation. This is in perfect agreement with the fact that no positive value is obtained for the activation
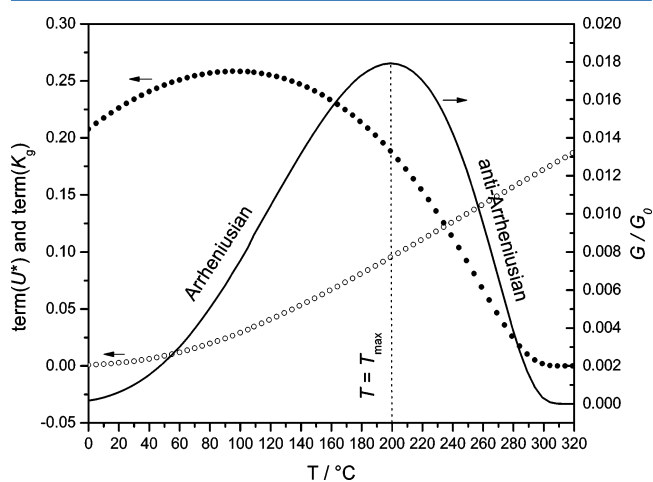

Figure 9. Schematic representation of the exponential terms contributing to the temperature dependence of linear growth rate G (eq 7). Line: G/G_0. Solid circles: term $(K_g) = \exp(-K_g/T\Delta Tf)$. Open circles: term $(U^*) = \exp(-U^*/R(T - T_\infty))$.

energy computed in the temperature range lying from 317 to 185 °C.

CONCLUSION

Crystallization of PTFE is so fast that it is difficult to observe it with optical microscopic measurements as well as isothermal and nonisothermal regular DSC measurements. A combination between DSC, FSC, and UFSC measurements has allowed studying the nonisothermal crystallization of PTFE for the first time over a wide range of cooling rates. It has been found that nucleation and crystal growth of PTFE occur only on cooling regardless of the cooling regime, as is the case for highly flexible polymers. It was impossible to outrun crystallization even for cooling rates approaching 800 000 K·s^{-1}. This attests for very fast homogeneous and heterogeneous nucleation processes which allow formation of PTFE crystals. Nevertheless, the crystallization process is affected under very fast cooling rate. Crystal size and perfection decrease progressively with increasing cooling rate, as suggested by the analysis of melting curves obtained after each undercooling. SEM observations confirm that only axialite crystals form under fast cooling, while a concentric arrangement of ribbon-like crystals is obtained at slow cooling rate. An advanced isoconversional method was applied to the crystallization of PTFE that highlights progressive transition from nucleation to a crystal growth controlled process. The study provides for the first time an advanced isoconversional analysis of PTFE crystallization kinetics over a large temperature domain using fast calorimetric data. Kinetic parameters obtained for crystallizations under low and high cooling rates were combined and fitted to the theoretical dependence of the growth rate derived from the Hoffman–Lauritzen theory. Application of this theory shows that the PTFE crystallization process shares the same dynamics on a very large time scale (from 10^{-4} to 10^3 s). It has never been demonstrated before with regular DSC or optical microscopy. Moreover, K_g values obtained for different portions of E_α dependency would indicate a transition from regime II to regime III. This is also the first time that such a transition in the kinetic regime is highlighted for PTFE.

AUTHOR INFORMATION

Corresponding Author
*E-mail: sbirrazz@unice.fr. Phone: +334 92 07 61 79. Fax: +334 92 07 61 19.

Notes
The authors declare no competing financial interest.

ACKNOWLEDGMENTS

REFERENCES

(1) Blanchet, T. A. *Plast. Eng.* **1997**, *41*, 981–1000.
(2) Biswas, S. K.; Vijayan, K. *Wear* **1992**, *158*, 193–211.
(3) Bunn, C. W.; Cobbold, A. J.; Palmer, R. P. *J. Polym. Sci.* **1958**, *28*, 365–376.
(4) Bassett, D. C.; Davitt, R. *Polymer* **1974**, *15*, 721–728.
(5) Rahl, F. J.; Evanc, M. A.; Fredericks, R. J.; Reimschuessel, A. C. *J. Polym. Sci., Part A-2* **1972**, *10*, 1337–1349.
(6) Price, D. M.; Jarratt, M. *Thermochim. Acta* **2002**, *392–393*, 231–236.
(7) Ozawa, T. *Bull. Chem. Soc. Jpn.* **1984**, *57*, 952–955.
(8) Wang, X. Q.; Chen, D. R.; Han, J. C.; Du, S. Y. *J. Appl. Polym. Sci.* **2002**, *83*, 990–996.
(9) Seo, Y. *Polym. Eng. Sci.* **2000**, *40*, 1293–1297.
(10) Lambrigger, M. *Polym. Eng. Sci.* **2004**, *44*, 2194–2202.
(11) Kostov, G.; Charadjiev, P.; Popov, A. *Eur. Polym. J.* **1993**, *29*, 1025–1029.
(12) Wang, Z.-C.; Kou, K.-C.; Chao, M.; Bi, H.; Yan, L.-K. *J. Appl. Polym. Sci.* **2010**, *117*, 1218–1226.
(13) Silvestre, C.; Cimmino, S.; Duraccio, D.; Schick, C. *Macromol. Rapid Commun.* **2007**, *28*, 875–881.
(14) Mileva, D.; Androsch, R. *Colloid Polym. Sci.* **2012**, *290*, 465–471.
(15) Zhuravlev, E.; Schmelzer, J. W. P.; Wunderlich, B.; Schick, C. *Polymer* **2011**, *52*, 1983–1997.
(16) Wurm, A.; Zhuravlev, E.; Eckstein, K.; Jehnichen, D.; Pospiech, D.; Androsch, R.; Wunderlich, B.; Schick, C. *Macromolecules* **2012**, *45*, 3816–3828.
(17) Kolesov, I.; Mileva, D.; Androsch, R.; Schick, C. *Polymer* **2011**, *52*, 5156–5165.
(18) Vyazovkin, S.; Burnham, A. K.; Criado, J. M.; Pérez-Maqueda, L. A.; Popescu, C.; Sbirrazzuoli, N. *Thermochim. Acta* **2011**, *520*, 1–19.
(19) Vyazovkin, S. *J. Comput. Chem.* **1997**, *18*, 393–402.
(20) Sbirrazzuoli, N.; Girault, Y.; Elégant, L. *Thermochim. Acta* **1997**, *293*, 25–37.
(21) Vyazovkin, S.; Sbirrazzuoli, N. *Macromol. Rapid Commun.* **2006**, *27*, 1515–1532.
(22) Vyazovkin, S. *J. Comput. Chem.* **2001**, *22*, 178–183.
(23) Sbirrazzuoli, N. *Macromol. Chem. Phys.* **2007**, *208*, 1592–1597.
(24) Vyazovkin, S.; Sbirrazzuoli, N. *J. Phys. Chem. B* **2003**, *107*, 882–888.
(25) Mathot, V.; Pyda, M.; Pijpers, T.; Vanden Poel, G.; van de Kerkhof, E.; van Herwaarden, S.; van Herwaarden, F.; Leenaers, A. *Thermochim. Acta* **2011**, *522*, 36–45.
(26) van Herwaarden, S.; Iervolino, E.; van Herwaarden, F.; Wijffels, T.; Leenaers, A.; Mathot, V. *Thermochim. Acta* **2011**, *522*, 46–52.
(27) Zhuravlev, E.; Schick, C. *Thermochim. Acta* **2010**, *505*, 14–21.
(28) Zhuravlev, E.; Schick, C. *Thermochim. Acta* **2010**, *505*, 1–13.
(29) Gradys, A.; Sajkiewicz, P.; Minakov, A. A.; Adamovsky, S.; Schick, C.; Hashimoto, T.; Saijo, K. *Mater. Sci. Eng., A* **2005**, *413–414*, 442–446.
(30) Khatipov, S. A.; Serov, S. A.; Sadovskaya, N. V.; Konova, E. M. *Radiat. Phys. Chem.* **2012**, *81*, 256–263.
(31) Papageorgiou, G. Z.; Achilias, D. S.; Bikiaris, D. N. *Macromol. Chem. Phys.* **2007**, *208*, 1250–1264.
(32) Ma, W.; Wang, X.; Zhang, J. *J. Therm. Anal. Calorim.* **2011**, *103*, 319–327.
(33) Hoffman, J. D.; Davis, G. T.; Lauritzen, J. I. *Treatise on Solid State Chemistry*; Hannay, N. B., Ed.; Plenum: New York, 1976; Vol. 3.
(34) Vyazovkin, S.; Sbirrazzuoli, N. *Macromol. Rapid Commun.* **2004**, *25*, 733–738.
(35) Lau, S. F.; Wesson, J. P.; Wunderlich, B. *Macromolecules* **1984**, *17*, 1102–1104.
(36) Oshima, A.; Ikeda, S.; Seguchi, T.; Tabata, Y. *Radiat. Phys. Chem.* **1997**, *49*, 581–588.
(37) Sauer, J. A.; Kline, D. E. *J. Polym. Sci.* **1955**, *18*, 491–495.
(38) Cheng, S. Z. D.; Janimak, J. J.; Zhang, A.; Cheng, H. N. *Macromolecules* **1990**, *23*, 298–303.
(39) Gan, Z.; Abe, H.; Doi, Y. *Biomacromolecules* **2000**, *1*, 704–712.
(40) Roitman, D. B.; Marand, H.; Miller, R. L.; Hoffman, J. D. *J. Phys. Chem.* **1989**, *93*, 6919–6926.
(41) Guigo, N.; Sbirrazzuoli, N.; Vyazovkin, S. *Soft Matter* **2012**, *8*, 7116–7121.
(42) Vyazovkin, S.; Dranca, I. *Macromol. Chem. Phys.* **2006**, *207*, 20–25.